Accelerated model-based quantitative diffusion MRI: A feasibility study for musculoskeletal application

Thomas Hüfken[1], **Jannik M. Arbogast**[1], **Anna-Katinka Bracher**[2], **Meinrad Beer**[2], **Henning Neubauer**[2,a], **Volker Rasche**[1,*,a]

[1] Department of Internal Medicine II, Ulm University Medical Center, Ulm, BW, Germany
[2] Department of Radiology, Ulm University Medical Center, Ulm, BW, Germany

Received 5 February 2021; accepted 13 April 2021

Abstract

Purpose: *To develop a model-based reconstruction technique for diffusion quantification based on accelerated two-dimensional echo planar data, obtained with multiple b-weightings. In combination with a dedicated undersampling pattern, acceleration factors above three were proven feasible in a clinical setting.*

Methods: *The proposed model-based method minimizes a cost function considering the l_2-norm of the difference between the Fourier transformation of a synthetic diffusion-model-generated k-space and the measured k-space data. Further regularization is performed by introduction of a total variation (TV) constraint to the cost function. Acceleration is achieved by a non-random undersampling pattern using acceleration factors that correspond to the total number of b-values. A rectangular region of variable size, centered in k-space, remains fully sampled for correction of phase variations, introduced by the different diffusion-encoding strengths.*

Results: *Qualitative analysis of the resulting images (S_0 and ADC) demonstrates the potential of the suggested undersampling pattern in combination with a model-based iterative reconstruction. An edge analysis highlights the preservation of high-frequency information for all investigated undersampling factors. In comparison to a conventional SENSE-accelerated reconstruction, the quantitative analysis of the ADC maps revealed a significantly ($P < 0.05$) superior performance of the suggested technique, enabling acceleration factors of $R = 3.65$ without compromising diffusion data fidelity.*

Conclusion: *The presented work shows the potential of model-based ADC quantification, which, in combination with a suited undersampling pattern for multiple b-values, enables more than three-fold acceleration using two-dimensional EPI without sacrificing ADC fidelity.*

Keywords: Diffusion, Model-based reconstruction, Iterative reconstruction, ADC

* Corresponding author: Volker Rasche, Department of Internal Medicine II, Ulm University, Albert-Einstein-Allee 23, 89081 Ulm, Germany.
E-mail: volker.rasche@uni-ulm.de (V. Rasche).
[a] Shared last authorship.

Z Med Phys **32** (2022) 240–247
https://doi.org/10.1016/j.zemedi.2021.04.004
www.elsevier.com/locate/zemedi

1 Introduction

Diffusion MRI is a non-invasive method commonly used to provide quantitative data on tissue diffusion properties. Diffusion weighted imaging (DWI) has already proven its potential as a valuable tool for neuroimaging, especially for stroke diagnosis [1] and in combination with diffusion tensor imaging (DTI) techniques, as basis for analysis of the structural connectivity in the brain [2]. Its role in musculoskeletal application is steadily increasing. Promising results by Barendregt et al. [3] indicate that DWI can replace contrast-enhanced MRI for diagnosing pediatric patients with juvenile idiopathic arthritis. Especially the role of the apparent diffusion coefficient (ADC) as an imaging biomarker of inflammation has been addressed [4]. However, the rather complex anatomy including bone, cartilage, muscle, fluid and others in combination with small structures pose challenges regarding scan time, while demanding accurate ADC quantification.

Obtaining quantitative diffusion information requires at least two images with different diffusion weightings per encoding direction. For accurate diffusion quantification, a series of images with increasing diffusion weighting is required. The rather long related acquisition times demand rapid acquisition methods, and echo-planar imaging (EPI) [5] has been established as quasi-standard in diffusion imaging. A major limitation of EPI arises from its sensitivity to artifacts like off-resonances or T_2^* induced image blurring [6], which often prevents the visualization of detailed structures. To mitigate these limitations, an increased bandwidth in the phase-encoded direction is needed, which is often realized by segmentation of the k-space applying multi-shot EPI techniques, where the k-space is filled using several subsequent excitations, often in combination with parallel imaging techniques [7].

Iterative reconstruction of images by minimization of a cost function is increasingly popular for the reconstruction of undersampled MR data. In case of a sparse representation of the MR data, and e.g. in combination with Compressed Sensing [8], further acceleration can often be achieved by solving a minimization problem, while ensuring data consistency under a certain data sparsity constraint such as a minimal total variation (TV). For quantitative MRI, it is possible to include detailed knowledge about the acquired data in form of a mathematical model in a cost function. This enables the direct estimation of quantitative maps without the need for intermediate images. Applications of model-based reconstructions have already been published for T_2 mapping [9,10], T_1 mapping [11,12], phase-contrast flow quantification [13,14] and diffusion [15–21] maps.

In this work, a diffusion model-based iterative reconstruction approach is combined with a total variation regularization and an echo-planar readout, including full consideration of the sensitivity properties of the multiple receive coils. However, motion and eddy-current-induced phase errors among excitations that are enhanced by the diffusion-sensitizing gradients, cause data inconsistencies and raise problems for the iterative reconstruction. While navigator echoes have been applied for respective phase corrections [17], we introduce an undersampling pattern that enables phase estimation from a fully sampled center region of k-space. Unlike other techniques our approach enables acquisition of multiple *b*-values by a specific undersampling of high frequency components. The suggested approach iteratively optimizes the initial magnetization and apparent diffusion coefficient maps as free variables of the cost function under full consideration of phase alterations between the different *b*-value images.

2 Methods

2.1 Model-based reconstruction

Diffusion encoding was performed by application of a Stejskal-Tanner [22] pulsed gradient spin echo preparation with a subsequent EPI readout. After a 90° excitation, diffusion sensitizing gradients were played out on either side of a 180° refocusing pulse. A series of images with different diffusion weightings *b* can be acquired and will show the well-known *b*-value related signal intensity decay $S(b)$, depending on the tissue-dependent diffusion coefficient D according to:

$$S(b) = S_0 \cdot e^{-b \cdot D} \tag{1}$$

with S_0 being the signal intensity resulting from no ($b = 0$) diffusion encoding. In clinical routine, an apparent diffusion coefficient (ADC) [23] is calculated by pixel-wise fitting a series of at least two *b*-values to Eq. (1). In this work, the ADC was calculated from diffusion data encoded along a single spatial dimension only.

Instead, the model-based approach compares the Fourier transform of a synthetic diffusion-model-generated k-space with the measured k-space data. Similar to Eq. (1), the model comprises an S_0 and ADC map. Both maps are matrices with $n_x \times n_y$ entries, as defined by the underlying imaging data, while the scalar b_i is the diffusion weighting of the i-th diffusion weighted image. Optimization of S_0 and ADC by minimization of the differences between the synthetic and measured diffusion weighted image series (dimension $n_x \times n_y \times n_b$) yields matrices with an anatomic (S_0) image and a respective ADC map.

The cost function ϕ consists of the l_2-norm of the difference between the synthetic and the measured k-space data $\tilde{S}_{i,c}(k)$, thus ensuring that the solution complies with the acquired k-space data as well as the expected *b*-dependent signal function.

The synthetic k-space is generated as follows:

$$y_{i,c}(S_0, \mathrm{ADC}) = A \cdot [C_c \circ S_0 \circ e^{-b_i \cdot \mathrm{ADC}}], \tag{2}$$

with $\circ$ denoting the Hadamard product (element-wise product), C_c being an $n_x \times n_y$ matrix providing the coil sensitivity

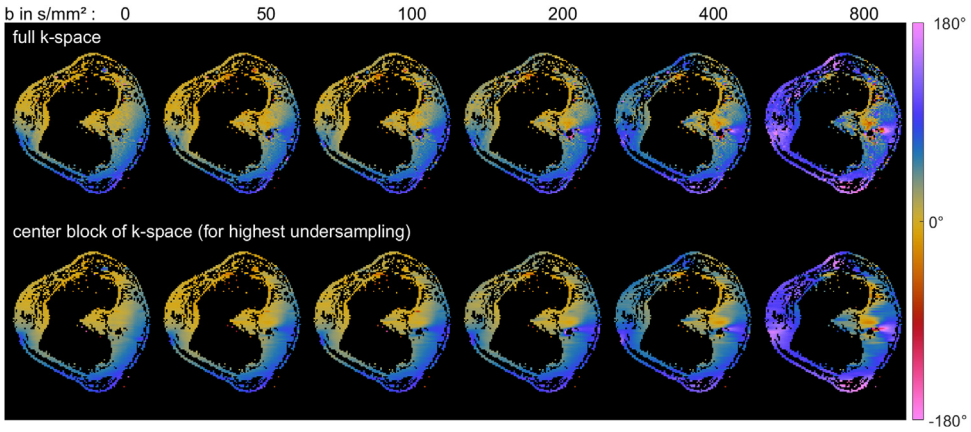

Figure 1. Phase P_i for the different b-values ranging from 0 to 800 s/mm^2. Phase maps in the upper row consider the full k-space, the ones in the second row only use 12.5% of k-space data, extracted from a block around the k-space center. A mask, generated with a threshold on a magnitude image, hides pixels of low SNR and clarifies the anatomy. Clear impact of the b-value (strength of diffusion weighting) on the phase can be appreciated. The phase is encoded according to the cyclic magenta-red-yellow-blue map described by P. Kovesi [27].

patterns for coil c and A being the Fourier operator. This yields an $n_x \times n_y \times n_b \times c$ synthetic k-space. During optimization, the final cost function value is calculated as the sum over the individual cost function values, calculated for each coil channel c and diffusion weighting i. As an additional regularization term, the l_1 norm of the total variation (TV) of the ADC map is used as constraint to enforce a piece-wise constant solution. The scalar regularization variable λ determines the relative weighting between the sparsity and the consistency term of the data as shown in Eq. (3). Appropriate settings of λ were derived manually by visual inspection of the resulting images. Since it is generally difficult to find an optimal λ, reconstructions with and without regularization are compared.

$$\phi\,(S_0, \mathrm{ADC}) = \frac{1}{2}\sum_i \sum_c \left\| y_{i,c}(S_0, ADC) - \tilde{S}_{i,c}(k) \right\|_2^2 + \lambda \|\mathrm{ADC})\|_1 \tag{3}$$

It is well known that phase alterations are introduced by strong diffusion gradients or by motion and need consideration during the reconstruction process. In our signal model, phase errors are taken into account by multiplying the model by a b-value dependent normalized phase matrix P with entries $p \in \mathbb{C}$ and $|p| = 1$. Since the phase is independent of the coil c, P is of size $n_x \times n_y \times n_b$. The final signal model function thus results in:

$$y_{i,c}(S_0, \mathrm{ADC}) = A \cdot [P_i \circ C_c \circ S_0 \circ e^{-b_i \cdot \mathrm{ADC}}]\,. \tag{4}$$

For the determination of the phase information, a special undersampling pattern was applied. As the phase varies smoothly, P can be approximated from a low-resolution image, derived from the central k-space lines (Figure 1). To ensure proper coverage of the k-space center, undersampling was limited to the outer regions of k-space (Figure 2). The undersampling factor R_o of the outer region results from the number of acquired b-values, which was set to $R_o = 6$ since 6 different b-values were used in the measurements. The overall retrospective undersampling factor R results from the different number of central k-space lines that are fully sampled, which were set to 50% ($R = 1.71$), 25% ($R = 2.67$), 16.6% ($R = 3.27$), and 12.5% ($R = 3.65$) of the total number of lines required for full k-space coverage. Between subsequently acquired b-values, the phase-encoding start position was shifted by Δk_y to ensure coverage of each k-space line once, when R_o equals the number of measured b-values. Thus, information about every frequency is contained in the undersampled data but weighted with different b-values. P was obtained from the phase of the low-resolution images, reconstructed from the fully sampled central section of k-space.

The minimization of the resulting cost function was achieved by iteratively applying a non-linear conjugated gradient (NLCG) algorithm, as presented by Hager and Zhang [24]. The gradients of the cost function were computed as provided in (Eq. (5)) with $\overline{(\cdot)}$ denoting the complex conjugate and $\Re\{\cdot\}$ the real part of the argument:

$$\begin{aligned}\frac{\partial \phi}{\partial S_0} &= \sum_{\mathrm{i}} \sum_{\mathrm{c}} e^{-b_i \cdot ADC} \\ &\circ \Re\left\{ \overline{P_i} \circ \overline{C_c} \circ \overline{A} \cdot \left[A \cdot \left(P_i \circ C_c \circ S_0 \circ e^{-b_i \cdot ADC} \right) - \tilde{S}_{i,c}\,(k) \right] \right\} \\ \frac{\partial \phi}{\partial ADC} &= \sum_i \sum_{\mathrm{c}} - b_i \cdot e^{-b_i \cdot ADC} \circ S_0 \\ &\circ \Re\left\{ \overline{P_i} \circ \overline{C_c} \circ \overline{A} \cdot \left[A \cdot \left(P_i \circ C_c \circ S_0 \circ e^{-b_i \cdot ADC} \right) - \tilde{S}\,(k) \right] \right\}\end{aligned} \tag{5}$$

To facilitate efficient convergence of the non-linear optimization, S_0 was initialized as the mean of the b_0-image, that was generated by combining b_0-images of different coils under consideration of the coil sensitivity maps. Further, the ADC-map was initialized with 0.0006 mm^2/s which has been

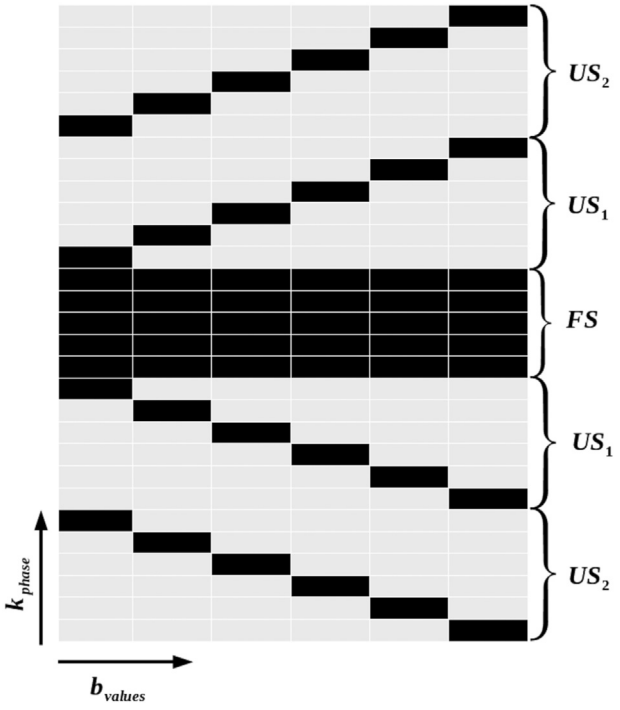

Figure 2. Undersampling pattern of the presented approach. Each entry in the matrix represents one line in read out direction. The phase encoding direction is shown vertical while the horizontal direction depicts the k-space for each of the six *b*-values. The outer regions (US_1 und US_2) in phase encoding direction are undersampled by a factor of $R_o = 6$, which corresponds to the number of measured *b*-values. The proportion of the fully sampled central block (*FS*) is varied to 1/2, 1/4, 1/6 and 1/8 of the complete k-space matrix, to generate different undersampling factors. Between subsequently acquired *b*-values, the outer undersampling pattern was shifted by one line in phase encoding direction to ensure coverage of each k-space line.

reported as lower boundary of the muscle diffusion coefficient [25]. The undersampling was performed retrospectively by an elementwise multiplication of the k-space with a mask. All reconstructions are based on the six different *b*-values (0, 50, 100, 200, 400, 800 s/mm^2).

2.2 Measurements

For evaluation of the feasibility of the suggested technique, non-undersampled diffusion data were acquired in nine healthy volunteers on a clinical MRI system (Achieva 3T, Philips Healthcare, Best, The Netherlands). All data were acquired using an eight-channel knee coil and a multi-shot diffusion weighted spin echo EPI technique. The scan parameters were: EPI-factor = 11, TE = 72.5 ms, TR = four heart phases, field-of-view FOV = 180 × 180 × 24 mm^3, voxel size $\Delta r = 1.3 \times 1.3 \times 5$ mm^3, 3 slices, slice gap: 4.5 mm, one average, *b*-values: 0, 50, 100, 200, 400, 800 s/mm^2. Electrocardiographic (ECG) triggering was applied to reduce blood flow artifacts especially from the popliteal artery.

2.3 Analysis

Resulting ADC values and corresponding standard deviations were quantified in the two regions of interest (ROIs) in the retropatellar cartilage and in the gastrocnemius muscle (see indicated areas in Figure 3B). Data derived from the suggested approach with different undersampling factors were compared with pixel-wise fitted images, obtained from complete data sets and respective undersampled data sets, individually reconstructed using SENSE. A pixel-wise non-accelerated ($R = 1$) reconstruction was used as reference.

For comparison of the resulting edge characteristics in ADC maps, an additional model-based reconstruction was performed based solely on the central k-space data. Quantification of edge broadening effects was performed on ADC intensity profiles, covering the transition from bone to cartilage to patella. For improving signal to noise ratio (SNR) three neighboring intensity profiles were averaged, and the result smoothed with a cubic spline interpolation. The full width at half maximum (FWHM) of the cartilage intensity was used for image-based quantification of structure broadening.

Statistical significance was assessed by applying an one-way analysis of variance (ANOVA) between the fully sampled reference, and the proposed model-based (with and without TV-regularization) and SENSE-based results for all investigated undersampling factors *R*. Additionally, Tukey's honestly significant difference procedure was used to identify significant differences between individual groups. ANOVA and Tukey were performed separately for the different ROIs. Differences were considered significant if $P < 0.05$.

3 Results

Reconstructed ADC maps of the human knee, derived from the different investigated reconstruction approaches for different *R* factors, are provided in Figure 3. From left to right, reconstructions with undersampling factors ranging from $R = 1$ to $R = 3.65$ (model-based reconstructions) and $R = 1$ to $R = 4$ (pixel-wise SENSE) are shown.

Best results for all reconstructions were obtained for $\lambda = 0.2$, yielding denoised S_0 images and ADC maps without any obvious regularization artifacts for all undersampling factors. The influence of different regularization parameters λ are presented as a supplemental material (supplement 1).

In the model-based reconstruction (Figure 3, row 1), the most obvious impact of undersampling on the resulting ADC maps is seen as increasing noise, which can be reduced by applying an additional TV regularization (row 2). In direct comparison to ADC maps, reconstructed from the fully sampled central k-space region only (row 3), the almost complete conservation of the image sharpness can be appreciated with and without TV regularization (row 1 and 2). The ADC maps

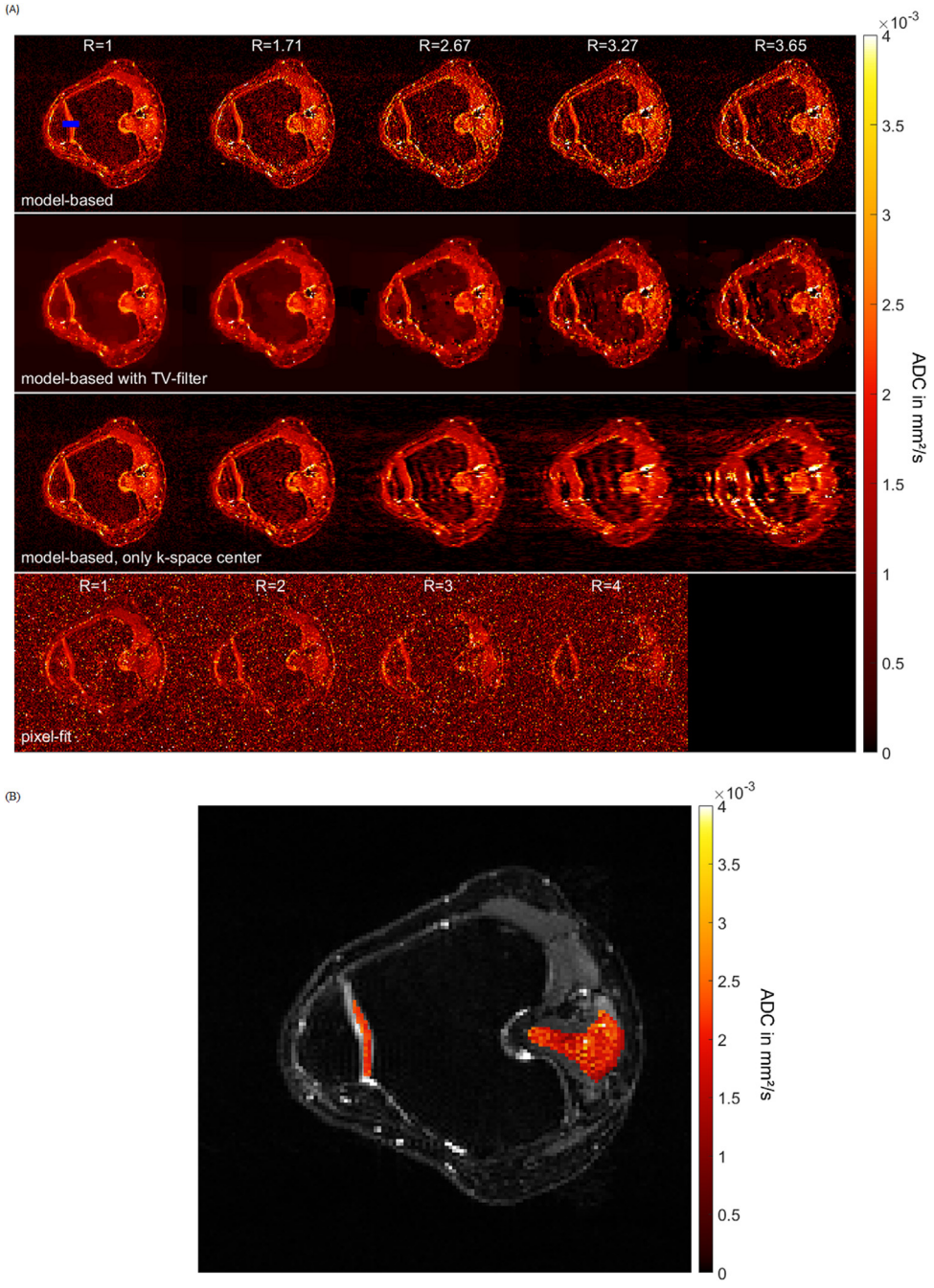

Figure 3. Results of the reconstructions with a left-right phase encoding direction and a linear colormap according to P. Kovesi [27], for the ADC values. A: reconstructed ADC-maps for different undersampling factors R (colums) and reconstruction techniques (rows). Model-based reconstructions without (row 1, row 3 (central k-space data only)) and with (row 2) TV-filter in direct comparison with the pixel-wise SENSE based reconstructions (row 4). The blue bar in row 1 indicates a profile for the investigation of structure broadening (Figure 4). B: S_0 image of the same volunteer with color coded overlay of ADC ROIs in the cartilage and the gastrocnemius.

using k-space center data only show obvious blur (row 3). This is confirmed by the quantitative assessment of edge sharpness, as demonstrated for one volunteer in Figure 4. The FWHM of the cartilage structure, based on nine volunteers, does increase with increasing undersampling from 6.5 ($R = 1$) to 12.4 ($R = 3.65$) pixels for ADC maps, derived from the central k-space region only. The cartilage width of reconstructions including outer k-space lines results in 6.5 ($R = 1$) to 7.5

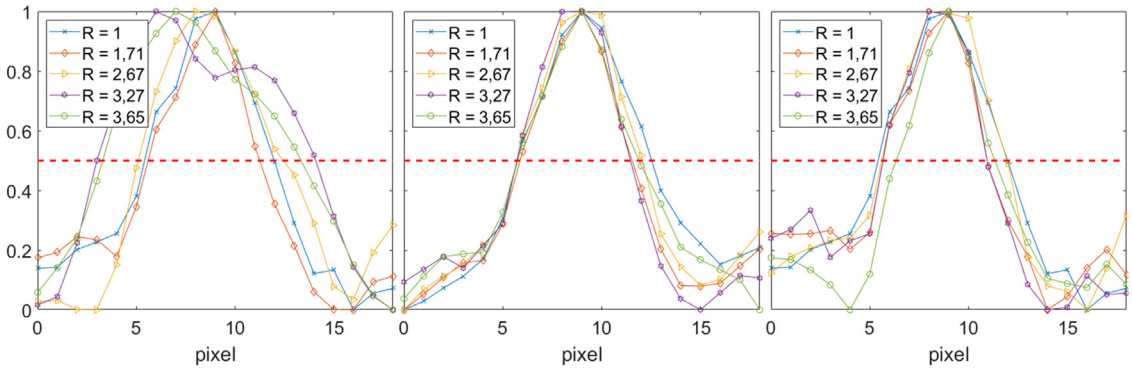

Figure 4. Cartilage width of one subject for different acceleration factors resulting from the suggested model-based iterative approach (left without and middle with TV regularization) and respective data reconstructed form the fully-sampled central k-space only.

($R = 3.65$) for reconstructions without TV and 6.7 ($R = 1$) to 6.9 ($R = 3.65$) pixels with TV regularization. Model-based reconstructions without TV regularization and $R = 1$ are presented in supplement 2 for all nine volunteers and in supplement 3 for different slices.

Direct comparison of the fully-sampled reference pixel-wise fitted mean ADC values and respective standard deviations, derived from the investigated undersampling approaches, are listed in Table 1. The mean ADC values of undersampled model-based reconstructions show differences compared to the reference with less than 20% (cartilage) and 5% (muscle) variation. The SENSE approach shows deviations of 57% (cartilage) and 44% (muscle). The combination of the cost function with a TV regularization mainly reduced the standard deviation in the ADC maps without any significant impact on the mean ADC values (less than 5%, compared to the same undersampling).

In general, decreased ADC values were observed with the SENSE approach causing significant differences already between non-accelerated ($R = 1$) SENSE and the fully-sampled reference, which was not observed with either of the model-based approaches for muscle tissue, but also in cartilage. Regarding undersampling ($R > 1$) no significant differences were observed between all acceleration factors for the model-based approaches. Even though significant differences between the reference and the SENSE reconstruction were observed for all acceleration factors, for $R \leq 3$ no significant differences were observed within the SENSE group. However, a further significant reduction was observed for $R = 4$.

4 Discussion

This work demonstrates the implementation and validation of a model-based reconstruction for quantitative diffusion imaging, representative for human knees. Especially for pediatric applications, the possible reduction in imaging time while maintaining ADC fidelity might further facilitate replacement of CA enhanced imaging. The presented model-based reconstruction algorithm uses the well-known diffusion related signal decay model to derive an estimate of S_0 and ADC from undersampled k-space data. For improving the apparent quality of ADC maps, the use of an additional regularization by TV has been shown.

Image phase is strongly dependent on the diffusion gradient strength and differs between different b-values. Such phase variations are difficult to consider during a model-based reconstruction, since the cost function itself and therefore its gradients (Eq. (5)) only yield real values. If not correctly considered, phase inconsistencies result in poor outcomes (supplement 4). In the proposed approach, such phase errors were considered by the introduction of a phase operator to the cost function.

The extraction of the phase information from undersampled k-space data was facilitated by the introduction of an undersampling pattern, which includes a fully sampled block around the k-space center. This allows the extraction of low-resolution phase maps, which were proven sufficient to reconstruct ADC maps without the loss of perceptible information, since the phase varies smoothly over the diffusion weighted images as shown in Figure 1.

Where reconstructions from the central block only yielded a broadening of the cartilage structure, with the proposed approach, acceleration factors of $R = 3.65$ still yielded a detailed reconstruction of the S_0 image as well as the ADC map. This can be appreciated in the ADC maps shown in Figure 3 as well as in the resulting broadening of the cartilage structure (Figure 4). A broadening of 5.9 pixels without using the high-frequency data during reconstruction can be reduced to below one pixel by adding the highly undersampled high-frequency k-space information. In addition, no artifacts were visible in the S_0 or ADC maps as might be expected due to the non-random undersampling pattern.

An advantage over pixel-wise computed ADC maps results from the suppression of noise in areas with low SNRs in the

Table 1
Mean ADC values from nine volunteers and standard deviations in the cartilage and muscle derived with different acceleration factors R for the model-based reconstruction (3000 iterations) with and without TV filter and for pixel-wise fitted maps.

Method	R	Muscle Mean	$[10^{-3}mm^2/s]$ Std	Cartilage Mean	$[10^{-3}mm^2/s]$ Std
Fully sampled (pixel-fit)	1	1.96	0.88	2.34	0.66
SENSE (pixel-fit)	1	1.60	0.46	1.68	0.17
	2	1.60	0.48	1.66	0.20
	3	1.53	0.60	1.64	0.39
	4	1.09	0.60	1.01	0.33
Model-based without TV	1	1.96	0.44	2.03	0.27
	1.71	1.93	0.53	1.97	0.32
	2.67	1.91	0.64	2.00	0.34
	3.27	1.93	0.68	2.01	0.35
	3.65	1.94	0.71	1.95	0.38
Model-based with TV ($\lambda = 0.2$)	1	1.94	0.27	1.99	0.17
	1.71	1.89	0.28	1.93	0.16
	2.67	1.87	0.35	1.91	0.18
	3.27	1.89	0.41	1.92	0.21
	3.65	1.90	0.46	1.88	0.22

diffusion weighted images (Figure 3). This advantage arises from Eq. (3), since the derivative of the cost function according to ADC is proportional to S_0. Due to this behavior, the cartilage appears clearly delineated in all ADC maps, which is degraded in pixel-wise fitted maps due to their noise amplitude in regions of low SNR.

Maybe even more important, quantitative ADC values (Table 1) were not significantly dependent on R with resulting relative variation of less than 8% for all investigated undersampling factors, while for the SENSE-based reconstruction with pixel-fit, a significantly larger variation, exceeding 25% for $R = 4$ was observed. The trend to lower ADC values with the SENSE and model-based approaches is still unclear and may need further attention.

Other groups like Bhagat et al.[26] have used SENSE-reconstructed diffusion weighted images with accelerations factors higher than 2. Pernicious reconstruction artifacts, such as aliasing and structural noise enhancement were apparent in the reconstructed ADC, thereby clearly limiting their use for a qualitative or quantitative analysis.

Where the additional regularization by applying a TV filter has no significant impact on the mean values in the two ROIs of the ADC map, it was successfully applied to reduce the standard deviation of the ADC in the investigated regions of interest. The superiority of model-based DTI in comparison to conventional Compressed Sensing has been shown for 3D Cartesian trajectories by Welch et al.[17] and for radial trajectories by Knoll et al.[18] Further Cartesian [15,16,19,21] (all retrospectively undersampled) and even a PROPELLER [20] readout have been reported demonstrating the advantages of a model-based DTI reconstruction from two different b-values for each direction. More details of published model-based DTI reconstructions are presented in the supplemental material (supplement 5). The presented approach uses six b-values in combination with an undersampling pattern that ensures coverage of each k-space line at least once with different b-weightings. This could be combined in a future work with an additional random undersampling, thereby improving the possible performance for Compressed Sensing, by furthermore enabling undersampling factors of $R \geq 4$, as recently presented e.g. by Dong et al. [19].

In its current form, the technique has been shown for EPI-like acquition schemes. The use of other non-Cartesian acquisition schemes like radial or spiral may even be more attractive due to the intrinsic oversampling of k-space as such yielding higher flexibility in providing low-resolution data for deriving the required phase information.

5 Conclusion

An iterative model-based reconstruction method for quantification of the ADC, using a dedicated non-random undersampling pattern, which enables the correction of phase variations over multiple diffusion weightings, was presented in this work. This model-based reconstruction has shown the potential to reconstruct undersampled diffusion data of knee joints with significantly improved data fidelity of the S_0 image and the ADC maps, compared to the well-established SENSE based pixel fit approach for undersampled k-space data.

Conflict of interest

The authors declare no conflict of interest.

Acknowledgements

This project has received funding from the German Research Foundation (Deutsche Forschungs gemeinschaft) DFG under grant agreement number 259187956 (NE 1953/1-1).

The authors thank the Ulm University Center for Translational Imaging MoMAN for its support.

Appendix A Supplementary data

Supplementary data associated with this article can be found, in the online version, at https://doi.org/10.1016/j.zemedi.2021.04.004.

References

[1] Schaefer PW, Grant PE, Gonzalez RG. Diffusion-weighted MR imaging of the brain. Radiology 2000;217:331–45.
[2] Jellison BJ, Field AS, Medow J, Lazar M, Salamat MS, Alexander AL. Diffusion tensor imaging of cerebral white matter: a pictorial review of physics, fiber tract anatomy, and tumor imaging patterns,. Am J Neuroradiol 2004;25:356–69.
[3] Barendregt AM, Mazzoli V, van Gulik EC, Schonenberg-Meinema D, Nassar-Sheikh al Rashid A, Nusman CM, et al. Juvenile idiopathic arthritis: diffusion-weighted MRI in the assessment of arthritis in the knee. Radiology 2020;295:373–80.
[4] Vendhan K, Bray TJP, Atkinson D, Punwani S, Fisher C, Sen D, et al. A diffusion-based quantification technique for assessment of sacroiliitis in adolescents with enthesitis-related arthritis. Br J Radiol 2016;89:20150775, http://dx.doi.org/10.1259/bjr. 20150775.
[5] Mansfield P. Multi-planar image formation using NMR spin echoes. J Phys C: Solid State Phys 1977;10:L55.
[6] Bernstein MA, King KF, Zhou XJ. Handbook of MRI pulse sequences. Elsevier; 2004.
[7] Pruessmann KP, Weiger M, Scheidegger MB, Boesiger P. SENSE: sensitivity encoding for fast MRI. Magn Reson Med 1999;42:952–62.
[8] Lustig M, Donoho D, Pauly JM. Sparse MRI: the application of compressed sensing for rapid MR imaging. Magn Reson Med 2007;58:1182–95.
[9] Hilbert T, Sumpf TJ, Weiland E, Frahm J, Thiran J-P, Meuli R, et al. Accelerated T2 mapping combining parallel MRI and model-based reconstruction: GRAPPATINI. J Magn Reson Imaging 2018;48:359–68.
[10] Block KT, Uecker M, Frahm J. Model-based iterative reconstruction for radial fast spin-echo MRI. IEEE Trans Med Imaging 2009;28:1759–69.
[11] Wang X, Kohler F, Unterberg-Buchwald C, Lotz J, Frahm J, Uecker M. Model-based myocardial T1 mapping with sparsity constraints using single-shot inversion-recovery radial FLASH cardiovascular magnetic resonance. J Cardiovasc Magn Reson 2019;21:60.
[12] Tran-Gia J, Wech T, Bley T, Köstler H. Model-based acceleration of Look-Locker T1 mapping. PLOS ONE 2015;10.
[13] Tan Z, Roeloffs V, Voit D, Joseph AA, Untenberger M, Merboldt KD, et al. Model-based reconstruction for real-time phase-contrast flow MRI: improved spatiotemporal accuracy. Magn Reson Med 2017;77:1082–93.
[14] Sun A, Zhao B, Li Y, He Q, Li R, Yuan C. Real-time phase-contrast flow cardiovascular magnetic resonance with low-rank modeling and parallel imaging. J Cardiovasc Magn Reson 2017;19:19.
[15] Zhu Y, Wu Y, Zheng Y, Wu EX, Ying L, Liang D. A model-based method with joint sparsity constraint for direct diffusion tensor estimation. In: 2012 9th IEEE international symposium on biomedical imaging (ISBI). 2012. p. 510–3.
[16] Zhu Y, Peng X, Wu Y, Wu EX, Ying L, Liu X, et al. Direct diffusion tensor estimation using a model-based method with spatial and parametric constraints. Med Phys 2017;44:570–80.
[17] Welsh CL, DiBella EVR, Adluru G, Hsu EW. Model-based reconstruction of undersampled diffusion tensor k-space data. Magn Reson Med 2013;70:429–40.
[18] Knoll F, Raya JG, Halloran RO, Baete S, Sigmund E, Bammer R, et al. A model-based reconstruction for undersampled radial spin-echo DTI with variational penalties on the diffusion tensor. NMR Biomed 2015;28:353–66.
[19] Dong Z, Dai E, Wang F, Zhang Z, Ma X, Yuan C, et al. Model-based reconstruction for simultaneous multislice and parallel imaging accelerated multishot diffusion tensor imaging. Med Phys 2018;45:3196–204.
[20] Cheryauka AB, Lee JN, Samsonov AA, Defrise M, Gullberg GT. MRI diffusion tensor reconstruction with PROPELLER data acquisition. Magn Reson Imaging 2004;22:139–48.
[21] Welsh CL, Hsu EW, DiBella EVR. Strategies for undersampling and reconstructing MR DTI data. In: 2011 IEEE international symposium on biomedical imaging: from nano to macro. 2011. p. 77–80.
[22] Stejskal EO, Tanner JE. Spin diffusion measurements: spin echoes in the presence of a time-dependent field gradient. J Chem Phys 1965;42:288–92.
[23] Le Bihan D, Breton E, Lallemand D, Grenier P, Cabanis E, Laval-Jeantet M. MR imaging of intravoxel incoherent motions: application to diffusion and perfusion in neurologic disorders. Radiology 1986;161:401–7.
[24] Hager WW, Zhang H. A new conjugate gradient method with guaranteed descent and an efficient line search. SIAM J Optim 2005;16:170–92.
[25] van Rijswijk CSP, Kunz P, Hogendoorn PCW, Taminiau AHM, Doornbos J, Bloem JL. Diffusion-weighted MRI in the characterization of soft-tissue tumors. J Magn Reson Imaging 2002;15:302–7, http://dx.doi.org/10.1002/jmri.10061.
[26] Bhagat YA, Emery DJ, Naik S, Yeo T, Beaulieu C. Comparison of generalized autocalibrating partially parallel acquisitions and modified sensitivity encoding for diffusion tensor imaging. Am J Neuroradiol 2007;28:293–8.
[27] Kovesi P. Good colour maps: how to design them; 2015.